

Impairing Factors in Remote-PPG Pulse Transit Time Measurements on the Face

Andreia Moço¹ Sander Stuijk¹ Mark van Gastel² Gerard de Haan²

¹Eindhoven University of Technology, Eindhoven, Netherlands

²Philips Research, Eindhoven, Netherlands

{a.moco, s.stuijk, m.j.h.v.gastel}@tue.nl, g.de.haan@philips.com

Abstract

The time it takes for a pulse wave to propagate between two arterial sites—i.e., the pulse transit time (PTT)—has received considerable attention as a marker of aortic stiffness and as a surrogate for blood pressure. However, obtrusiveness and manual intervention requirements render conventional PTT measurement methods inappropriate for ubiquitous monitoring. In this regard, high-speed camera systems are interesting alternatives. Recognizably, a technical breakthrough would be estimating PTT with a relatively inexpensive RGB camera pointed at the face only. A simple means to do this is determining the phase shift (PS) between photoplethysmographic (PPG) signals extracted at collocated skin pixels. In this paper, we show that the validity of this approach is threatened by skin variability. We analysed simultaneous video recordings of the neck and face in 21 subjects (ages, 33 ± 11 yrs). These were used to extract PPG signals at the face and skin motion (sMOT) signals at the vicinity of the carotid artery. Using sMOT as reference signal, we show that the pressure wave undergoes delay and frequency leakage as it propagates across the arterial tree; the extent of propagation distortion is subject-dependent and place PPG-based estimations at a disadvantage in comparison with PTTs measured at the arterial level. Awareness is further raised for the site-dependency of PS outcomes by the provision of facial PPG-phase maps and collocated PPG signals. Lastly, impairments due to waveform dissimilarity are demonstrated under exercise-induced PTT changes. In conclusion, PS is unsuitable for PTT measurements at the face.

1. Introduction

Pulse transit time (PTT) is the time it takes for the pressure or flow wave to propagate between two arterial sites [8]. PTT responds to changes of the arterial elastic modulus [24, 4] and, when measured invasively, correlates well with blood pressure (BP) [2, 3, 10]. Reduced PTTs are symptomatic of hypertension and of arterial stiffening [12]. For

standardization purposes and inter-subject comparisons of aortic stiffness, transit times are usually converted to the corresponding pulse wave velocities (PWV) measurements. PWV along big arteries is particularly interesting as an independent risk factor of cardiovascular diseases [30]. Non-invasive PWV estimates are typically obtained by arterial applanation tonometry; with subjects in supine position, assessments of the pressure wave are made by gently compressing mechanotransducers or piezoelectric sensors over the skin covering superficial sections of the carotid, radial or femoral arteries (see Fig. 1) [26].

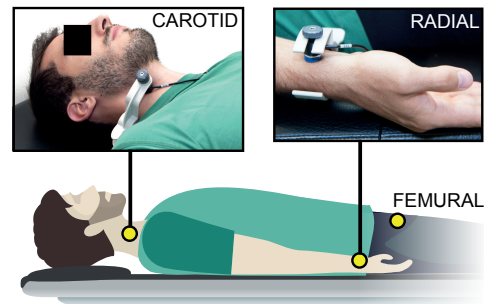


Figure 1. Typical body sites for applanation tonometry recordings. The PTT between the carotid and femoral pressure waves is used to obtain reference measurements of aortic PWV, though the radial artery may also be used for distal measurements.

Pulse pressure waveforms obtained by applanation tonometry are similar to invasive measurements [25], but it is also possible to detect the arrival of the pressure waves by measurement modalities which sense arterial vessel wall motions as skin motion (sMOT) signals. Examples include laser-speckle patterns [11], optical vibrocardiography (VCG) [22] and, more recently, camera-based VCG methods [33, 17, 1]. It is perhaps the selection of measurement sites and methodology that determine the validity and prognostic value of PWV/PTT measurements. For example, radial pressure waveforms may be easily recorded but the brachial artery does not reflect the atherosclerotic process as extensively as the arteries of the lower limb [11, 5].

This is why gold standard measurements of aortic PWV, as index of aorta stiffening [25], involve measuring the wave foot delay from carotid-femoral pressure recordings. Unfortunately, carotid tonometry is difficult in patients with thick necks, uncomfortable and may dislodge the carotid plaque. Also, motion and waveform artifacts are a known issue in applanation tonometry [25]. These drawbacks, combined with the ongoing pursuit of non-obtrusiveness and cost-efficiency in cardiovascular health monitoring, have motivated active research in contactless PPG-based PTT methods (hereafter referred to as PPG-PTT methods), in particular with the ultimate goal of measuring BP ubiquitously [23, 7, 14, 28].

PPG-PTT methods aim at determining the relative delay between proximal and distal arterial waveforms [38]. Measurements are often performed between the R-peaks of ECG traces and the onset of PPG waveforms at peripheral body sites, e.g., finger [37]. Nevertheless, this approach confounds actual PTT values with the pre-ejection period (PEP) of the heart [15]. Replacing ECG by a proximal PPG sensor solves the problem and creates interesting prospects for camera-based systems [23, 27]. However, PPG-based methods come with the inherent disadvantage that the timing of PPG waveforms may not coincide with the pressure waveforms due to viscoelastic delays introduced by the skin microvasculature [23]. The extent by which this possible source of error impairs PPG-PTT estimates is, at the time being, unclear [16]; contributions in this regard are key for further progress on contactless PPG-PTT monitoring.

To the best of our knowledge, the magnitude of skin effects in PPG-PTT estimates has only been assessed in response to probe pressure [29]. Likewise, the feasibility of estimating PTT based on the PSs between PPG signals from the face only, or by combining face-peripheral sites, have not been investigated in-depth. If it can be shown that facial PPG signals suffice for continuous PWV/PTT monitoring, then measurement requirements may be relaxed to accommodate various body postures and find application in non-clinical settings. A convenient scenario for single-site PPG-PTT methods is shown in Fig. 2, featuring a subject in seated position and a camera for remote acquisition of proximal-distal pairs of PPG signals, which are processed for determining PTT based on PS measurements.

In this paper, we use the neck-face as case-study and assess the waveform changes between sMOT and PPG signals. To do this, we use camera-based PPG and VCG frameworks [17, 18] for extracting these signals, separately. The waveform deformation across the vasculature are then modeled using transfer functions (TFs) for amplitude and phase responses at multiples of the pulse-rate frequency. These TFs allow a compact inspection of skin variability effects in PPG-PTT measurements. The invariance of the TFs to subject-specific and skin-surface effects would suffice to

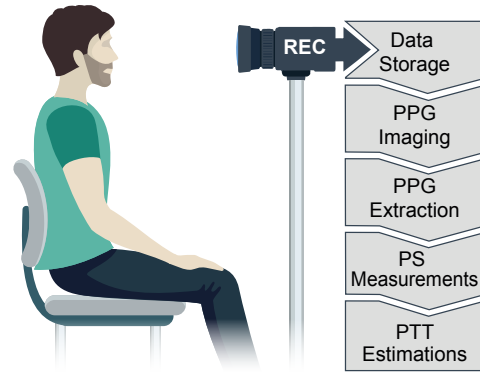


Figure 2. Scenario for contactless PTT measurements.

support that PPG-PTT measurements can be as accurate as those based on signal modalities aiming major arteries (e.g., sMOT or applanation tonometry signals). In the remainder of this paper, we will show that this is not the case; waveform dissimilarities at the face are clearly seen and overshadow PTT-related effects in the PS metric. We shall also show that actual PTT changes can be confounded by changes of the morphological dissimilarity between proximal and distal waveforms.

The remainder of this manuscript is as follows. The next section describes our imaging and signal processing approach. Results are provided in Section 3 and discussed in Section 4. Concluding remarks are found in Section 5.

2. Methods

2.1. Propagation distortions across the arterial tree

This section aims to model the deformation from sMOT to PPG in green. Conceptually, these signals are modulated differently, but share origin at pulse pressure variations. sMOT signals occur under uneven lighting conditions and are mostly modulated by cardiac-related angular displacements of the skin surface with respect to the incident light flux [20]. At the skin-surface spots covering superficial sections of the common carotid artery, the temporally varying and AC/DC-normalized sMOT signals can be expressed as a summation of a carotid displacement term; PPG signal at the light wavelength, λ ; and sensor noise, n [17]. Formally,

$$sMOT(t) = f[d_{CA}(t)] + PPG_{\lambda} + n(\lambda, t). \quad (1)$$

The function $f[\cdot]$ translates tissue-induced deformations between carotid wall movements, d_{CA} , and skin displacements. For non-obese individuals, the superficial adipose tissue at the neck is not thick and $f[\cdot]$ may be assumed to be linear. We remark that a calibration from displacement to aortic/central pressure waveforms would also be possible, though exceeding the scope of this investigation [32]. By

measuring sMOT signals using red (R) wavelengths, the interference of PPG_λ can be neglected [17] and the expression for sMOT simplifies to

$$sMOT(t) \approx C d_{CA}(t) + n_R(t), \quad (2)$$

with constant $C \in \mathbb{R}$. Complementarily, PPG signals extracted using green wavelengths are modulated by blood volume variations at the level of upper dermal arterioles [18]. PPG signals are easily contaminated by movements, but the problem can be addressed by subtracting normalized signals in green, PPG_{Gn} , and red, PPG_{Rn} . Similar to [6], we refer to this mapping as GminR. Because PPG_{Gn} is much stronger than PPG_{Rn} , the shape of PPG_{GminR} is fairly equivalent to the (unpolluted) PPG_{Gn} and is similarly “dampened” by the microvascular bed of tissue.

A Windkessel model is used for describing the deformation of PPG_{GminR} w.r.t. sMOT (see Fig. 3). Propagation effects are accounted for by including capacitor-resistance elements for charging during systole and for discharging during diastole. Local variations are translated as parametric changes of the electrical elements. The non-homogeneity of the microvascular beds (particularly the uneven proximity to arteries) ultimately results in waveform dissimilarities between PPG_{GminR} waveforms extracted at collocated sites. Since transit times within the face are in the order of 1–10 ms, one may expect that even minor skin variations suffice to interfere with and mask actual PTT effects in the PS between PPG_{GminR} pairs.

The discharging resistance is fairly large, which is realistic for healthy subjects. The circuits can be compacted further into a low-pass-filter (LPF) equivalent for the cutaneous impedance, with sMOT and PPG_{GminR} as its input and output signals, respectively. We assume no venous pulsations, which seems reasonable in measurements performed at or above the heart level [13].

2.2. Data acquisition

Dataset We used data from 21 subjects (ages, 23 to 62 yrs, 33 ± 11 yrs; SBP/DBP, $12.0 \pm 1.5 / 7.1 \pm 0.4$; 3 females) recruited for [17]. The selection criteria was visibility of the cheek and neck, and amplitude of sMOT signals at least as high as that of PPG signals. An informed consent was obtained from each subject and the study was approved by the Internal Committee Biomedical Experiments of Philips Research.

Setup and protocol The experimental setup was designed for joint camera-based acquisition of facial PPG_{GminR} and sMOT signals. All video recordings contain the neck and cheek. Six of these video recordings also contain the forehead. Subjects sat on a chair (with back and head support; recumbent position, 70 degrees with respect to the horizon-

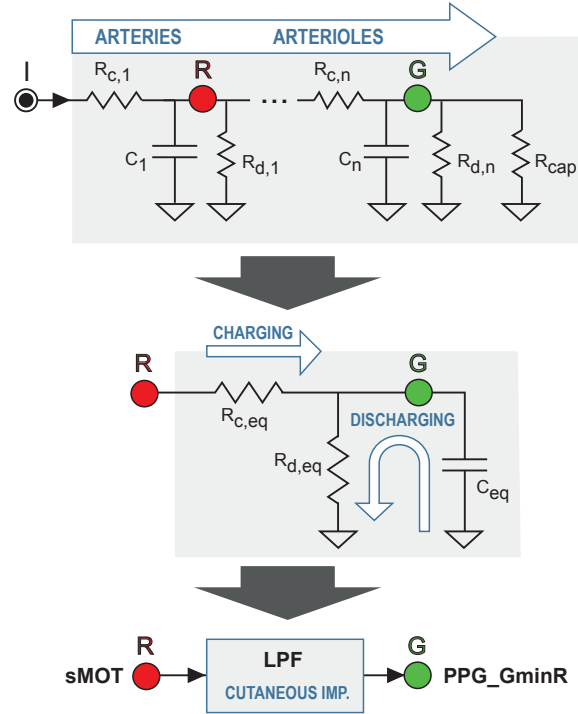


Figure 3. A Windkessel model for describing the propagation distortion undergone by pulsatile pressure waves across the arterial tree and its effect in the morphological dissimilarity between sMOT and PPG_{GminR} signals. sMOT signals are extracted using red wavelengths probe arterial displacements, whereas PPG_{GminR} signals are modulated by dermal arterioles.

tal plane) and were instructed to breath normally and avoid voluntary movements.

We configured a regular RGB camera (global shutter RGB CCD camera USB; model, UI-2230SE-C, IDS, Germany; frame sizes, 700×400 pixels or 500×500 pixels; resolution, 8 bit depth) for data acquisition at a constant frame rate of 30 Hz. Recordings were stored in an uncompressed bitmap format. Uneven illumination conditions for the neck were created using two fluorescent lamps (Philips, model HF3319/01). These are dimmable and equipped with an internal AC power supply at 22 kHz, which prevents interference with the camera frame rate. Synchronized with video recordings, contact-PPG signals (cPPG) were acquired by finger pulse oximetry attached to right index finger (model CMS50E, Contec, China). cPPG signals were used for probing the instantaneous pulse-rate during recordings and served as a reference for mapping the pulsatile strength of surface neck motion.

The same equipment was used for performing an additional measurement of the forehead and palm of three subjects in the supine position. Homogeneous illumination was used for optimal PPG signal acquisition, whereas specular reflections were mitigated by using a cross-polarization

scheme (implemented by covering the light sources and camera lens with linear polarizing film). Simultaneously, ECG and cPPG signals were acquired for computing the pulse arrival time (PAT). Subjects were instructed to have their faces static during 2 minutes of rest, followed by a 1-minute-long isometric handgrip contraction (left hand) with the aim of inducing a PAT reduction.

2.3. Signal processing

Stream pre-processing All video frames (red and green channel; original sizes 500×500 or 768×576 pixels) were blurred with a Gaussian kernel (box size, 45×45 pixels) and resized by a factor of 1/5–1/6, resulting in images of size 100×100 pixels or 128×96 . For invariance to brightness intensity, displacement signals were converted from raw least significant bit (l.s.b.) format to normalized AC/DC-amplitude [31].

VCG imaging The local strength of skin-surface micromotion was inspected by camera-based VCG imaging [17]. Accordingly, the VCG-motion amplitude maps were obtained by taking the complex inner-products between a two-dimensional array of normalized displacement-streams at the neck-surface and a reference cPPG signal (synchronously acquired). These maps guided us at demarcating suitable a skin region of interest (sRoI) for querying sMOT in the vicinity of the carotid artery (see Fig. 4(c)). To minimize PPG interference, VCG maps were based solely on the red camera channel.

PPG imaging We computed separate maps for the PPG_{Gn} and PPG_{Rn} signal streams. By subtracting these from one another, we obtained amplitude and phase maps of PPG_{GminR} [18]. PPG signals were extracted at cheeks, forehead and palm.

Ensemble-averaging To obtain representative waveforms for sMOT and PPG_{GminR} signals for each subject, we ensemble-averaged (EA) cardiac cycles as described in [17]. EA-waveforms were scaled in amplitude to unity and temporally registered to a template of 35 samples per cardiac cycle.

Describing propagation effects We employed TFs to describe propagations distortions between: sMOT and PPG_{GminR} at the cheek and/or forehead; between PPG_{GminR} signals extracted at the cheek and forehead; and between PPG_{GminR} signals from the forehead and palm. To this end, analytic source and output signals, s and y , respectively, were first created by replicating the sMOT and PPG_{GminR} waveforms 100 times. The TFs were modeled, separately for each subject, as linear filters, w . Accordingly,

$$PPG_{GminR} \approx w * sMOT, \quad (3)$$

where $*$ denotes convolution. w was estimated as follows:

$$\mathbf{T} = \Gamma[s] \quad (4)$$

$$\mathbf{C}_s = \mathbf{T}^T \cdot \mathbf{T} \quad (5)$$

$$w = \text{pinv}[\mathbf{C}_s] \cdot (\mathbf{T}^T \cdot y) \quad (6)$$

where the operator $\Gamma[\cdot]$ denotes the formation of the Toeplitz matrix from the source vector s , and truncation to its 10 first columns. With w configured for having 20 taps, \mathbf{T} has size 3500×20 , while its covariance matrix, \mathbf{C}_s , is 20×20 . The Matlab command *freqz* was used to compute the amplitude and phase responses of w in the frequency domain (i.e., Bode plots). Of relevance are the responses at multiples of the pulse-rate frequency.

Pulse arrival times (PAT) Reference PAT measurements were performed as the temporal offsets between R-peaks in ECG data and systolic peaks in cPPG signals acquired at the finger. The obtained PAT points were spline-smoothed using the MATLAB function *smoothn* [9].

3. Results

3.1. Deformation across the arterial tree

An investigation of morphological changes between sMOT and facial PPG signals begins with the demarcation of rRoIs for extracting these signals. In this regard, it is useful to observe Fig. 4, which contains sample frames and imaging outcomes from a representative subject from our dataset. Suitable sRoIs for sMOT and PPG signal extraction are indicated in the red and green sample frames shown in Fig. 4(a) or Fig. 4(b). The availability of amplitude maps is particularly advantageous for demarcating sMOT, as this location is clearly evidenced as hotspot in the VCG-motion amplitude map computed (see Fig. 4(c)).

The extracted signals are exemplified in Fig. 5 after AC/DC-normalization. sMOT and PPG_{GminR} signals are periodic and have clear systolic peaks. More importantly, it is seen that the shape of PPG_{GminR} seems delayed w.r.t. sMOT. Similar observations hold in the remaining dataset.

The sensor noise in sMOT and PPG_{GminR} signals can be easily overcome in EA-waveform representations. The improved resolution is clearly seen in Fig. 6(a). Converting EA-waveforms to the frequency domain further indicates that the signal content is mostly within the first third harmonics of the pulse-rate frequency (see Fig. 6(b)). Subsequent analyses will be conducted in this harmonic range.

Figure 7 shows the obtained TF between the EA-waveforms for sMOT and PPG_{GminR} , evidencing that the harmonic components of PPG_{GminR} signals are delayed

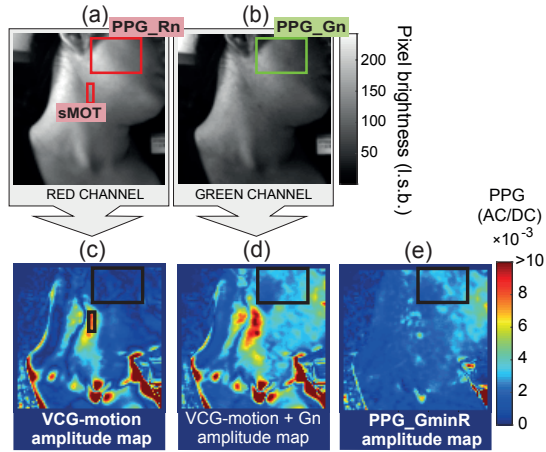


Figure 4. Representative neck-face recording and imaging outcomes, including (a,b) manually-defined sROIs for sMOT over the carotid artery and facial PPG_{GminR} acquisition. The sROI demarcation is assisted by inspecting the (c) VCG and the (e) PPG_{GminR} amplitude maps, respectively [Subject 12].

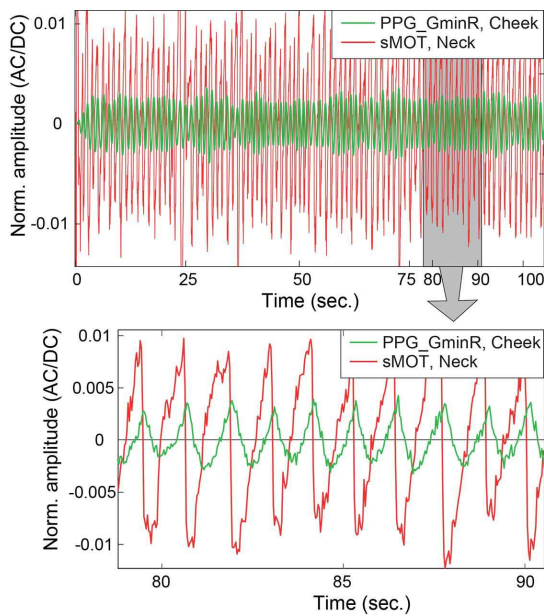


Figure 5. Periodicity and morphological heterogeneity between AC/DC-normalized sMOT and PPG_{GminR} signals [Subject 12].

w.r.t. its sMOT counterparts by more than 100 degrees (see yellow flag in Fig. 7). This corresponds to about 8 samples on a template of 35 samples per cardiac cycle. This delay is illustrated explicitly for the first harmonics of the signals; i.e., as PSs between sine waves.

To support the representativeness of the above TF, Fig. 8 shows the mean and 95% limits of agreement (LoAs) for the full dataset. The low-pass-filtering response confirms that the terminal arterial tree is a distortive media which

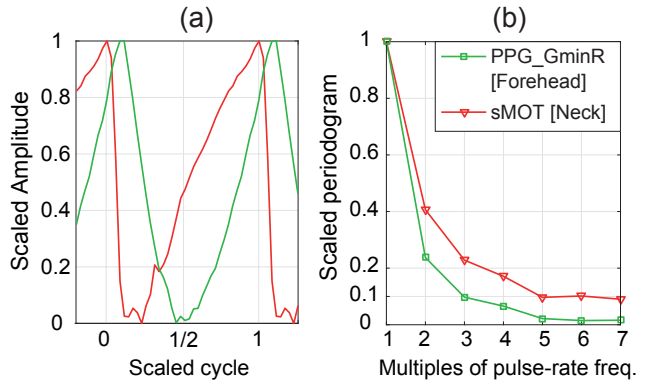


Figure 6. (a) sMOT and PPG_{GminR} EA-waveforms, and (b) the corresponding amplitude spectra, indicating harmonic content leakage for PPG w.r.t. sMOT signals [Subject 12].

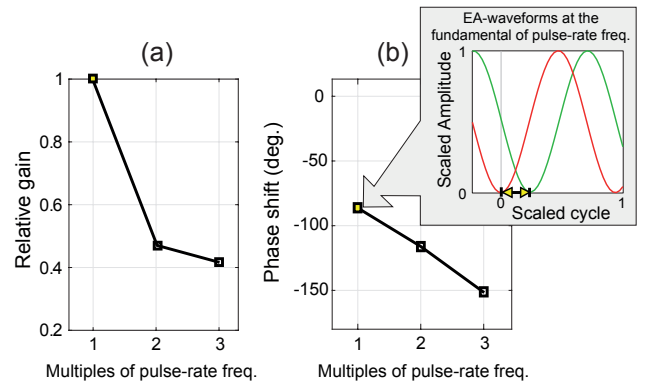


Figure 7. Transfer functions (TFs) from sMOT (carotid artery) to PPG_{GminR} signals, evidencing (a) the low-pass-filtering profile of the skin tissue; and (b) linear phase delay w.r.t. the first harmonics of the pulse-rate frequency [Subject 12].

introduces leakage of harmonic content.

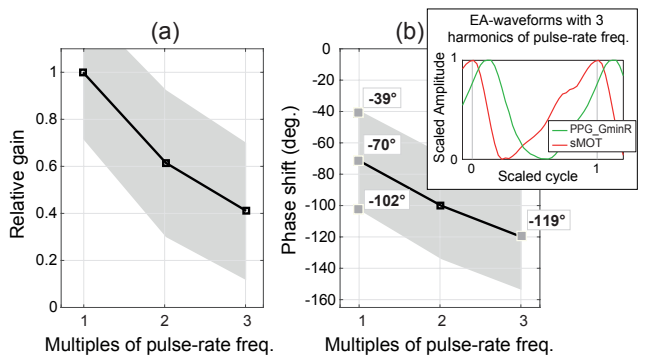


Figure 8. Average TFs from sMOT (input) to PPG_{GminR} signals, indicating (a) harmonic content leakage, and (b) relative delays for the first multiples of the pulse-rate frequency. The gray area indicates 95% limits of agreement.

LoAs are also wide for PS responses (about ± 30 degrees for the three first harmonics), meaning that inter-individual effects indeed impair the accuracy of PPG_{GminR}-PTT based estimates w.r.t. reference PTT measurements (obtained by arterial displacements or tonometry measurements).

For a number of subjects, simultaneous recordings of sMOT and PPG_{GminR} at the cheek and forehead were also performed. Figure 9 refers to one of such recordings. Clearly, the magnitude of PSs and distortion effects are less pronounced between PPG_{GminR} signals acquired at two facial skin sites (cheek-input; forehead-output) than between sMOT and facial PPG_{GminR}.

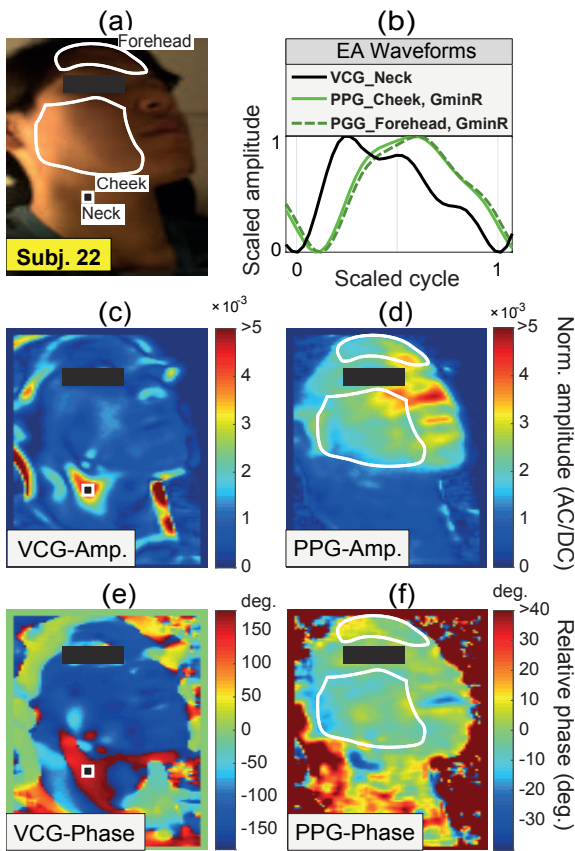


Figure 9. Comparing sMOT and PPG_{GminR} signals at the face (cheek and forehead). VCG and PPG imaging assist in selecting sROIs and evidence the non-homogeneity of PSs within the face.

These initial insights were confirmed in the TFs of five additional subjects. As seen in Fig. 10, the PSs between the fundamental harmonics of sMOT and PPG_{GminR} signals are within 50–100 degrees, whereas PSs between cheek-forehead PPG_{GminR} signals do not exceed 20 degrees. The apparent stability of single-modality comparisons of PSs seems favorable for single-site measurements. However, the inter-individual differences between TFs may impair calibration attempts from PSs from facial measurements.

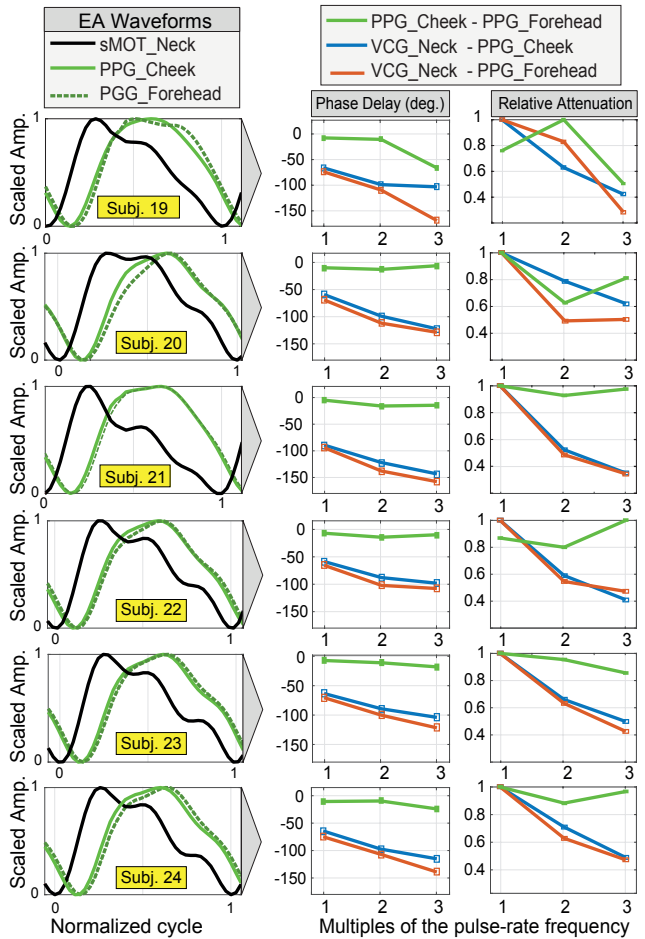


Figure 10. TFs between sMOT and PPG_{GminR} signals extracted at the forehead and right cheek [Subjects 19-24].

3.2. Mapping the PPG-Phase at the forehead

We assessed the potential accuracy of single-site PPG-phase-based PTT measurements by inspecting the forehead in detail. Figure ??(a) depicts the forehead of a subject in supine position. Figures 11(b,c) show the amplitude and relative phases maps of PPG_{GminR}, and indicate that the local PSs on the forehead is variable. Regional variations within 10 degrees are easily observed, in particular near superficial arteries (e.g., supratrochlear artery).

The phase of PPG_{GminR} signals within the forehead (with an sROI as indicated in Fig. 11) is 5.0 ± 4.5 degrees. For comparison, a similar inspection for PPG_{Gn} and PPG_{Rn} signals indicates larger phasic variabilities (7.4 ± 10.2 and 1.2 ± 5.7 for PPG_{Gn} and PPG_{Rn}, respectively), which are likely be due to motion contamination.

The same subject was instructed to perform an isometric handgrip exercise, following 2 minutes of rest. Figure 12 shows the measured PAT and PPG waveforms acquired at the forehead, cheeks and palm. Note that PPG_{GminR} wave-

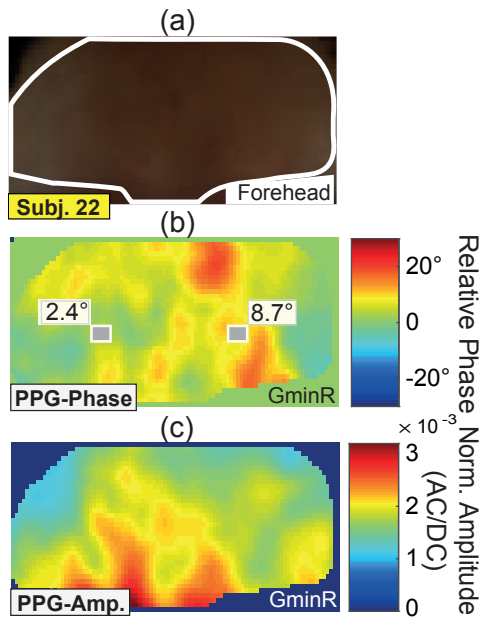


Figure 11. Amplitude and phase maps of PPG_{GminR} at the forehead, evidencing significant surface variations of PSs which are caused by the proximity to superficial arteries [subject 19].

Periods	PS _{Rn}	
	forehead-palm	cheek-forehead
Rest	25.2°	14.8°
Exercise	6.3°	17.5°

Periods	PS _{GminR}	
	forehead-palm	cheek-forehead
Rest	30.3°	12.5°
Exercise	28.8°	14.4°

Table 1. PSs between PPG_{GminR} and PPG_{Rn} signals acquired before and during an handgrip exercise intervention (denoted as PS_{Rn} and PS_{GminR}, respectively) [Subject 19].

forms barely change at facial signals with exercise. Conversely, PPG_{Rn} clearly change

Table 1 lists PS measurements performed between PPG_{Rn} and PPG_{GminRn} signals, during rest and exercise. PSs were calculated between forehead and palm (fp), and between forehead and cheek (fc). Although differences of almost 20 degrees are seen for PPG_{Rn}-fp, these are due to morphological differences between proximal and peripheral signals (see yellow flags indicated in PPG_{Rn}-palm in Fig. 12, rather than PPT. The confounding effect of morphological differences in PSs were observed in two additional subjects for PPG_{Rn}. Effects under GminR were not systematically observed.

Table 1 contains PS measurements between signals truncated to the fundamental of the pulse-rate. However, similar observations hold for signals truncated to three harmonics (absolute differences are below 3°).

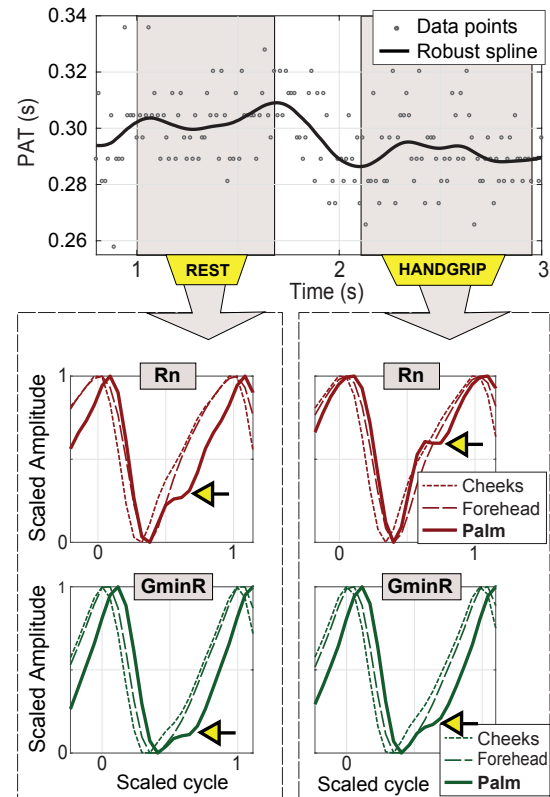


Figure 12. Effect of exercise on the PAT and waveform shapes of PPG signals acquired at the chin, forehead and palm. [Subject 19].

4. Discussion

PTT reflects aortic stiffness and has been identified as surrogate for non-invasive BP monitoring [23]. Recognizing the technical advantage of measuring PPT with a regular RGB camera and, preferably, from the face only, we investigated pitfalls of PPG-PTT methods based on the PS metric. The attractiveness of this approach resides in its simplicity, relative ease of computation and applicability in ambulatory scenarios. In particular, we explored the extent by which skin-variability effects impair the performance PPG-PTT outcomes. To this end, we started by estimating the TFs from sMOT (over the carotid artery) to facial PPG_{GminR} signals in a dataset of mostly young male subjects.

Our results suggest that the arterial tree and its termination at the microvascular beds of tissue delay and low-pass-filter the pulse pressure wave, resulting in waveform dissimilarities between sMOT and PPG_{GminR}. Yet, the extent of deformation varies across individuals. For example, the average PSs between sMOT and PPG_{GminR} in our dataset was about 70 degrees at the fundamental of the pulse-rate frequency. The 95% LoAs were as wide as ± 30 degrees, which is a source of error in PPG-PTT methods. Interesting insights were also obtained by investigating the PSs mea-

sured between facial skin sites. In this regard, the PPG-phase images extracted at the forehead suffice to evidence skin-variability errors in PS calculations. With the size of forehead sRoIs being only about 10 per 5 cm, skin-surface variations in the range of 5 degrees preclude PPG-PTT measurements under GminR mappings. The large inter-individual variations at the TFs from cheek to forehead also suggest this impossibility.

Additional insights from induced PAT/BP changes suggest that, in addition to being “polluted” by skin-surface effects, the PS metric confounds the morphological dissimilarity between proximal and distal waveforms with actual PTT effects. Stated another way, both the actual PTT/PWV and the dissimilarity between PPG or sMOT waveform pairs may change jointly and non-linearly. This is understood in light of the fact that BP increases are usually accompanied by increased elasticity of the arterial vessels through vasodilation mechanisms [21].

We believe that our insights are valuable for establishing the applicability scope of PPG-phase-imaging to anatomical description of the skin perfusion status, and, possibly, as indication of the surface-dependency of deformations of the pulse-pressure wave. Future work may explore the morphological aspects of sMOT and/or PPG signals for deriving PPT or BP estimations, although our described impairing factors in intrinsic to camera-based measurements and holds for methodological approaches beyond the PS metric. In fact, recent works indicate the feasibility of retrieving PTT or BP directly from waveforms by training neural networks in datasets of finger pulse oximetry [36] or radial pressure waveforms [34, 35].

Limitations Firstly, we acknowledge the fact that our sample consists of mostly young, healthy male individuals. Diversifying the dataset, particularly in terms of age and BP, can lead to expanded LoAs of the TFs. In terms of methodological design, we acknowledge the inherent drawback of sMOT signals as indirect measure of carotid displacements. Albeit small, the damping effect introduced by the neck tissue, as well as possible shape variations of the pulse pressure wave along the common carotid artery, add to the observed variability of the observed inter-subject LoAs at the obtained TFs. The availability of paired recordings of invasive measurements of the carotid pulse pressure and facial PPG signals would improve this study. Furthermore, we remark that red and green wavelengths interrogate the skin at different depths, leading to morphological differences between signals. Since the skin is spatially inhomogeneous, the mixing of wavelengths in the GminR operation is a possible additional factor contributing to spurious phase measurements and to impaired PTT estimations at the face [18]. Still, the contribution of normalized green PPG is dominant and the incurred error of performing the GminR

operation is preferable to not correcting for motion artifacts [19]. Lastly, we note that the sampling period of the camera (~ 33 ms) is within the range of PTT and affects the precision of timing measurements.

5. Conclusion

The extent of inter-individual variability in the deformation between sMOT and PPG_{GminR} is indicative of a disadvantage of PPG w.r.t. sMOT signals for deriving accurate PS or PTT measurements. Our results also indicate that the PS between proximal-distal PPG signals reflects PTT to a lesser extent than skin non-homogeneities. Furthermore, the fluctuations of PTT can be accompanied by changes in the relative dissimilarity between PPG waveforms, hence complicating the relation between PS and PTT. Thus, the PS between PPG signals is an unreliable metric for measuring PTT, irrespective of whether the signals are extracted at the face only or between face and palm.

ACKNOWLEDGMENT

We express our gratitude to Dr. Wim Verkruijsse and Dr. Marc Op de Beeck from Philips Research, the Netherlands, for revising the manuscript. In addition, we thank Tang Tang and Luis Z. Mondragon, from the Eindhoven University of Technology, for their contributions to this paper.

References

- [1] R. Amelard, R. L. Hughson, D. K. Greaves, K. J. Pfisterer, J. Leung, D. A. Clausi, and A. Wong. Non-contact hemodynamic imaging reveals the jugular venous pulse waveform. *Sci. Rep.*, 7:40150, 2017. **1**
- [2] H. C. Bazett and N. B. Dreyer. Measurements of pulse wave velocity. *Am. J. Physiol.-Legacy Content*, 63(1):94–116, 1922. **1**
- [3] D. Bergel. The static elastic properties of the arterial wall. *J. Physiol*, 156(3):445–457, 1961. **1**
- [4] Y. Chen, C. Wen, G. Tao, M. Bi, and G. Li. Continuous and noninvasive blood pressure measurement: a novel modeling methodology of the relationship between blood pressure and pulse wave velocity. *Ann Biomed Eng*, 37(11):2222–2233, 2009. **1**
- [5] J. I. Davies and A. D. Struthers. Pulse wave analysis and pulse wave velocity: a critical review of their strengths and weaknesses. *J. Hypertens*, 21(3):463–472, 2003. **1**
- [6] G. de Haan and V. Jeanne. Robust pulse-rate from chrominance-based rPPG. *IEEE Trans. Biom. Eng*, 60(10):2878–2886, 2014. **3**
- [7] M. De Melis, U. Morbiducci, L. Scalise, E. P. Tomasini, D. Delbeke, R. Baets, L. M. Van Bortel, and P. Segers. A noncontact approach for the evaluation of large artery stiffness: a preliminary study. *Am. J. Hypertens*, 21(12):1280–1283, 2008. **2**
- [8] M. Gao, N. B. Olivier, and R. Mukkamala. Comparison of noninvasive pulse transit time estimates as markers of blood

- pressure using invasive pulse transit time measurements as a reference. *Physiol. Rep.*, 4(10):e12768, 2016. 1
- [9] D. Garcia. Robust smoothing of gridded data in one and higher dimensions with missing values. *Comput. Stat. Data Anal.*, 54(4):1167–1178, 2010. 4
- [10] L. A. Geddes, M. H. Voelz, C. F. Babbs, J. D. Bourland, and W. A. Tacker. Pulse transit time as an indicator of arterial blood pressure. *Psychophysiology*, 18(1):71–74, 1981. 1
- [11] M. Golberg, J. Ruiz-Rivas, S. Polani, Y. Beiderman, and Z. Zalevsky. Large-scale clinical validation of noncontact and continuous extraction of blood pressure via multipoint defocused photonic imaging. *Appl. Opt.*, 57(7):45–51, 2018. 1
- [12] B. Gribbin, A. Steptoe, and P. Sleight. Pulse wave velocity as a measure of blood pressure change. *Psychophysiology*, 13(1):86–90, 1976. 1
- [13] M. Hickey, J. P. Phillips, and P. A. Kyriacou. Investigation of peripheral photoplethysmographic morphology changes induced during a hand-elevation study. *J. Clin. Monit. Comput.*, 30(5):727–736, 2015. 3
- [14] I. C. Jeong and J. Finkelstein. Introducing contactless blood pressure assessment using a high speed video camera. *J. Med. Syst.*, 40(4):77, 2016. 2
- [15] C. S. Kim, A. M. Carek, R. Mukkamala, O. T. Inan, and J. O. Hahn. Ballistocardiogram as proximal timing reference for pulse transit time measurement: Potential for cuffless blood pressure monitoring. *IEEE Trans. Biomed. Eng.*, 62(11):2657–2664, 2015. 2
- [16] S. Loukogeorgakis, R. Dawson, N. Phillips, C. N. Martyn, and S. E. Greenwald. Validation of a device to measure arterial pulse wave velocity by a photoplethysmographic method. *Physiol. Meas.*, 23(3):581–596, 2002. 2
- [17] A. Moço, L. Z. Mondragon, S. Sander, and G. de Haan. Camera-based assessment of arterial stiffness and wave reflection parameters from neck micro-motion. *Phys. Meas.*, 2016. 1, 2, 3, 4
- [18] A. Moço, S. Sander, and G. de Haan. Skin inhomogeneity as a source of error in remote PPG-imaging. *Biom. Opt. Express*, 7(11):4718–4733, 2016. 2, 3, 4, 8
- [19] A. Moço, S. Stuijk, and G. de Haan. Motion robust PPG-imaging through color channel mapping. *Biomed. Opt. Express*, 7(5):1737–1754, May 2016. 8
- [20] A. Moco, S. Stuijk, and G. de Haan. Ballistocardiographic artifacts in PPG imaging. *IEEE Trans. Biom. Eng.*, 63(9):1804–1811, 2016. 2
- [21] S.-H. Moon, J.-C. Moon, D.-H. Heo, Y.-H. Lim, J.-H. Choi, S.-Y. Kim, K.-S. Kim, and S.-J. Joo. Increased pulse wave velocity and augmentation index after isometric handgrip exercise in patients with coronary artery disease. *Clin. Hypertens.*, 21:5, 2015. 8
- [22] U. Morbiducci, L. Scalise, M. De Melis, and M. Grigioni. Optical vibrocardiography: a novel tool for the optical monitoring of cardiac activity. *Ann. Biomed. Eng.*, 35(1):45–58, 2007. 1
- [23] R. Mukkamala, J. Hahn, O. T. Inan, L. K. Mestha, C. Kim, H. Treyin, and S. Kyal. Towards ubiquitous blood pressure monitoring via pulse transit time: Theory and practice. *IEEE Trans. Biom. Eng.*, 62(8):1879–1901, 2015. 2, 7
- [24] D. L. Newman and S. E. Greenwald. *Validity of the Moens-Korteweg Equation*, pages 109–115. Springer Berlin Heidelberg, Berlin, Heidelberg, 1978. 1
- [25] M. F. O’Rourke and A. Adji. An updated clinical primer on large artery mechanics: implications of pulse waveform analysis and arterial tonometry. *Curr. Opin. Cardiol.*, 20(4):275–281, 2005. 1, 2
- [26] T. Pereira, C. Correia, and J. Cardoso. Novel methods for pulse wave velocity measurement. *J. Med. Biol. Eng.*, 35(5):555–565, 2015. 1
- [27] J. Proenca, J. Muehlsteff, X. Aubert, and P. Carvalho. Is pulse transit time a good indicator of blood pressure changes during short physical exercise in a young population? *Conf. Proc. IEEE Eng. Med. Biol. Soc.*, 2010:598–601, 2010. 2
- [28] A. Secerbegovic, J. Bergsland, P. S. Halvorsen, N. Suljanovic, A. Mujcic, and I. Balasingham. Blood pressure estimation using video plethysmography. In *Proc. ISBI*, pages 461–464. IEEE, 2016. 2
- [29] X. F. Teng and Y. T. Zhang. The effect of contacting force on photoplethysmographic signals. *Physiol. Meas.*, 25(5):1323, 2004. 2
- [30] C. The Reference Values for Arterial Stiffness. Determinants of pulse wave velocity in healthy people and in the presence of cardiovascular risk factors: “establishing normal and reference values”. *Eur. Heart J.*, 31(19):2338–2350, 2010. 1
- [31] W. Verkruyse, L. O. Svaasand, and J. S. Nelson. Remote plethysmographic imaging using ambient light. *Opt. Express*, 16(26):21434–21445, 2008. 4
- [32] S. J. Vermeersch, E. R. Rietzschel, M. L. De Buyzere, D. De Bacquer, G. De Backer, L. M. Van Bortel, T. C. Gillebert, P. R. Verdonck, and P. Segers. Determining carotid artery pressure from scaled diameter waveforms: comparison and validation of calibration techniques in 2026 subjects. *Physiol. Meas.*, 29(11):1267–1280, 2008. 2
- [33] H. Wu, M. Rubinstein, E. Shih, J. Guttag, F. Durand, and W. Freeman. Eulerian video magnification for revealing subtle changes in the world. *ACM Trans. Graph.*, 31(4), 2012. 1
- [34] H. Xiao, M. Butlin, I. Tan, A. Qasem, and A. Avolio. Estimation of pulse transit time from radial pressure waveform alone by artificial neural network. *IEEE J. Biomed. Health Inform.*, 2017. 8
- [35] H. Xiao, A. Qasem, M. Butlin, and A. Avolio. Estimation of aortic systolic blood pressure from radial systolic and diastolic blood pressures alone using artificial neural networks. *J. Hypertens.*, 35(8):1577–1585, 2017. 8
- [36] X. Xing and M. Sun. Optical blood pressure estimation with photoplethysmography and FFT-based neural networks. *Biom. Opt. Express*, 7(8):3007–3020, 2016. 8
- [37] Y. Yoon, J. H. Cho, and G. Yoon. Non-constrained blood pressure monitoring using ecg and ppg for personal healthcare. *J. Med. Syst.*, 33(4):261–266, 2009. 2
- [38] C. C. Young, J. B. Mark, W. White, A. DeBree, J. S. Vender, and A. Fleming. Clinical evaluation of continuous noninvasive blood pressure monitoring: accuracy and tracking capabilities. *J. Clin. Monit.*, 11(4):245–252, 1995. 2